Dynamics of postnucleation and domain growth: Domain-spatial correlation function

Tao Huang, Tomohiro Tsuji, M. R. Kamal, and A. D. Rey
Department of Chemical Engineering, McGill University, 3610 University Street, Montreal, Quebec, Canada, H3A 2B2
(Received 27 January 1998)

Postnucleation and domain growth have been investigated by direct imaging of real-time *in situ* observation in semicrystalline polymer films. The pattern evolution and spatiotemporal dynamics are conducted with the domain-spatial correlation function $G(r,t)$, which we reported briefly in a previous study [Phys. Rev. E **58**, 789 (1998)]. In this paper we present the general definition of the domain-spatial correlation function for stochastic droplet systems and an interpretation for typical liquidlike and solidlike structures in physics systems. The application of the domain-spatial correlation function and an extensive analysis on simultaneous nucleation, continuous nucleation, multiple nucleation, and growth processes have been reported with experimental data. The domain-spatial correlation function directly yields the time-dependent domain-size distribution function and the spatial correlation function of domain core centers simultaneously throughout the entire process, including the postnucleation, domain growth, and grain formation stages. The scaling relation $\mathcal{G}(r/R_g(t))=G(r,t)/G(r=0,t)$, where $R_g(t)$ is the location of the first minimum of $G(r,t)$, has been defined and evaluated from experimental data. It is exact for free growth during the postnucleation stage and it also provides a basis for the interpolation between the impingement stage and grain structures. Furthermore, we indicate that the domain-spatial correlation function and the direct imaging program are useful tools and suitable to characterize any static droplet patterns and dynamic processes in a wide range of scientific fields. [S1063-651X(98)09311-8]

PACS number(s): 64.60.Qb, 64.70.Dv, 68.55.−a, 81.30.−t

I. INTRODUCTION

The domain growth and evolution of spatial structures have long received attention in various fields of science [1,2]. The domain growth associated with first-order nonequilibrium phase transformations occurs by spinodal decomposition or nucleation and growth [3,4]. Reasonable agreement between scattering experiments and theory for phase separation and ordering has been achieved for many different materials. In contrast, there are many unsolved problems in nucleation growth. Although Kolmogorov, Johnson, Mehl, and Avrami's (KJMA's) [5] theory of nucleation and growth predicts the time dependence for the reacted fraction, it does not provide any information on the domain-size distribution. The classical theoretical treatment of the dynamics of a nucleation and growth system is based on the growth of nuclei that are larger than a certain ''critical size'' [6–8]. Experimental results on nucleation and growth in mixtures of low-molecular-weight compounds [9], colloidal suspensions [10], and polymer blends [11,12] are in qualitative disagreement with classical theory. Recently, a phase-field model and simulation of kinetics of polymorphous crystallization of an amorphous solid have been proposed, which consider the coupling of a nonconserved local lattice structure and a conserved local atomic composition [13].

The kinetic studies of first-order phase transitions have been devoted to the characterization and evaluation of correlation functions and their relationship with time-dependent diffraction studies. The time-dependent spatial correlation and structure factor have been extensively used in studying the phase ordering kinetics [3]. Sekimoto [14] evaluated an exact expression of the two-point correlation functions, provided the domain-size distribution is known, which is also related to the crystallized fraction. In n dimensions, it was deduced by Ohta *et al.* [15] under certain restrictions. The evaluation of the correlation functions in this system has usually been performed by means of the time-core method. Axe and Yamada [16] obtained an expression of the grain autocorrelation function in the case of a one-dimensional system and constant nucleation rate and growth velocity based on Kolmogorov's model. In this case, the universal domain-size distribution is obtained for $t\rightarrow 0$. However, due to the lack of isotropy of the one-dimensional case, the results obtained cannot be generalized to higher dimensions. Again, they did not consider spatial correlation, which is another very important structural measure for any kind of domain growth or ordering. In the two-dimensional case, the grain autocorrelation function was estimated by Monte Carlo simulation. Scaling was found for $t\rightarrow 0$ and it is no longer exact in the late stages of growth. Finally, Axe and Yamada extended the scaling assumption and suggested using it for diffraction studies. Unfortunately, they did not present any experimental data. Actually, to our knowledge, no experimental data of this kind have been published until now.

In this work we choose polymer as a model system to study nucleation and growth. There are several advantages to studying nucleation-growth phenomena during the postnucleation stage using semicrystalline polymer films. Polymeric materials look more complicated at first sight than small molecular materials; however, for polymeric systems many collective length scales are very large and hence a phenomenological (quasiuniversal) description is much more appropriate. With respect to kinetic phenomena at first-order

phase transitions, the characteristic time scale of relaxation and diffusion of polymeric macromolecules is much slower than for small molecular materials. Due to this slow dynamics of polymer crystallization, deeper quench or larger supercooling ($\Delta T = T_m - T_c \gg 1 \sim 10\ ^\circ\mathrm{C}$) is needed for normal nucleation and growth, so the small thermal fluctuations have less effect on the system. The nucleation and growth of polymeric materials is interface kinetics controlled and growth ($\sim 10^{-3} - 10\ \mu$m/sec) is much slower than in diffusion controlled systems, so higher resolution in time and space can be easily achieved. In addition, the nucleation rate, linear growth velocity, and geometrical shape of domain growth (polymer spherulites) are easily characterized [17]. Also, experimental observation shows that spherulitic domains grow independently of each other and there is neither Ostwald ripening nor elastic long-range interactions during the nucleation and growth process. The above features of the post-nucleation and growth of polymer spherulitic domains simplify the experimental measurements and theoretical analysis.

The pattern evolution and spatiotemporal dynamics are conducted with the domain-spatial correlation function $G(r,t)$, which was discussed briefly in previous studies [18]. In this paper we present the general definition of the domain-spatial correlation function for stochastic droplet systems and an interpretation for typical liquidlike and solidlike structures in physics systems. The application of the domain-spatial correlation function and an extensive analysis on simultaneous nucleation, continuous nucleation, multiple nucleation, and growth processes have been reported with experimental data. We also develop a method using the time-resolved digital imaging analysis to investigate domain growth. The experimental results have been obtained for nucleation growth in semicrystalline polymer films.

The organization of this paper is as follows. In Sec. II we present the general definition of the domain-spatial correlation function (DSCF) for stochastic droplet systems. In Sec. III we develop an algorithm and software to compute the DSCF. We present the evaluation of a static domain-spatial correlation function and an interpretation for typical liquidlike and solidlike structures in physics systems. In Sec. IV we propose a theoretical model of nucleation and growth in terms of a dynamic domain-spatial correlation function. In Sec. V the application of the domain-spatial correlation function and an extensive analysis on simultaneous nucleation, continuous nucleation, multiple nucleation, and growth processes have been reported with experimental data. A scaling relation is defined and evaluated using experimental data. The experimental findings and conclusions are summarized in Sec. VI.

II. DOMAIN-SPATIAL CORRELATION FUNCTION

Definition of the domain-spatial correlation function

Consider a droplet domain pattern $\Omega(\vec{\mathbf{x}}_1, \vec{\mathbf{x}}_2, \ldots, \vec{\mathbf{x}}_N)$, where $\vec{\mathbf{x}}_i$ is the position vector for point i within Ω. In order to fully describe the structure of the droplet domain pattern, we introduce a domain-spatial correlation function to probe the geometric domain-size distribution and spatial correlation of the system simultaneously. The order parameter $\psi(\vec{\mathbf{x}})$ and a number density operator $\Phi(\vec{\mathbf{x}})$ are defined as

$$\psi(\vec{\mathbf{x}}) = \begin{cases} 1 & \text{if } \vec{\mathbf{x}} \in \text{the droplet domain} \\ 0 & \text{if } \vec{\mathbf{x}} \in \text{the rest space outside droplet domains,} \end{cases} \tag{1}$$

$$\Phi(\vec{\mathbf{x}}) = \left\langle \sum_{i=1}^{n} \delta(\vec{\mathbf{x}} - \vec{\mathbf{x}}_i) \right\rangle, \tag{2}$$

where $\vec{\mathbf{x}}$ is the position vector, angular brackets denote the average over the ensemble, and $\delta(\vec{\mathbf{x}})$ is the Dirac δ function.

To define the domain-spatial correlation function, the system can be treated as the combination of two groups of elements: the droplet domains and the domain–core-center points. By adopting the definition of partial time-space correlation function [19], we obtain the n-point partial correlation function

$$\left[\frac{1}{\Re}\int \psi(\vec{\mathbf{x}},t)\,d\vec{\mathbf{x}}\right]^{n-1} G^{(n)}(\vec{\mathbf{x}}^{(n)},t) = \left\langle \frac{\Phi^{(n)}(\vec{\mathbf{x}}^{(n)},t)}{\prod_{k=1}^{n} \Phi^{(1)}(\vec{\mathbf{x}}_k,t)} \prod_{k=1}^{n} \psi(\vec{\mathbf{x}}_k,t) \right\rangle, \tag{3}$$

where $G^{(n)}(\vec{\mathbf{x}}^{(n)},t)$ is the n-point partial correlation function of the domain-core centers and the domains, $(1/\Re)\int \psi(\vec{\mathbf{x}},t)\,d\vec{\mathbf{x}}$ is the domain density, $\Re$ is the system geometry measure, $\Phi^{(n)}(\vec{\mathbf{x}}^{(n)},t)$ is the grand canonical n-particle density, and $\Phi^{(1)}(\vec{\mathbf{x}}^{(n)},t)$ is the one-point particle density. The term $\Phi^{(n)}(\vec{\mathbf{x}}^{(n)},t)/\Pi_{k=1}^{n}\Phi^{(1)}(\vec{\mathbf{x}}_k,t)$ gives the joint probability density to find a droplet at position $(\vec{\mathbf{x}}_1, \vec{\mathbf{x}}_2, \ldots, \vec{\mathbf{x}}_N)$ at times t. The term $\Pi_{k=1}^{n}\psi(\vec{\mathbf{x}}_k,t)$ is the probability of finding one of the points $\vec{\mathbf{x}}_1, \vec{\mathbf{x}}_2, \ldots, \vec{\mathbf{x}}_N$ inside any droplet domain at the respective times $t_1, t_2, \ldots, t_N$.

Let us denote $P_s([\Phi],t)$ as the time-dependent probability distribution of the field Φ and $P_d(r - \Sigma_{k,j;k\neq j}^{n} |\vec{\mathbf{x}}_k - \vec{\mathbf{x}}_j|, t; r, dr, \tau, d\tau)$ as the probability that all of the positions $\vec{\mathbf{x}}_1, \vec{\mathbf{x}}_2, \ldots, \vec{\mathbf{x}}_n$ at the respective times $t_1, t_2, \ldots, t_n$ may appear in the region $r\,dr$ during the time interval $[\tau, \tau + d\tau]$. $G^{(n)}(\vec{\mathbf{x}}^{(n)},t)$ can be expressed as follows:

$$G^{(n)}(r,t)=\left[\frac{1}{\Re}\int\psi(\vec{\mathbf{x}},t)d\vec{\mathbf{x}}\right]^{-(n-1)}\times\left\langle\int D[\Phi]P_s([\Phi],t)\prod_{k=1}^{n}\Phi(r-|\vec{\mathbf{x}}_k-\vec{\mathbf{x}}_j|,t)\prod_{r}\prod_{\tau}P_d\left(r-\sum_{k,j;k\neq j}^{n}\left|\vec{\mathbf{x}}_k-\vec{\mathbf{x}}_j\right|,t;r,dr,\tau,d\tau\right)\right\rangle, \tag{4}$$

where $D[\ ]$ is a differential operator. Alternatively, the static two-point domain-spatial correlation function can be expressed according to Eqs. (1)–(3) as

$$G(r)=\left(\frac{1}{\Re}\int\psi(\vec{\mathbf{x}})d\vec{\mathbf{x}}\right)^{-1}\left\langle\sum_{k}^{N}\int\delta(r-|\vec{\mathbf{x}}_k-\vec{\mathbf{x}}|)\psi(\vec{\mathbf{x}})d\vec{\mathbf{x}}\right\rangle. \tag{5}$$

The domain-spatial correlation function for the two-dimensional case $G_i(r)$, for an arbitrarily chosen domain i with $\vec{\mathbf{x}}_i$ as the origin of the domain core center, is defined by counting the domains whose position vectors lie within a distance dr from a circle of radius r with center at the origin at time t, which yields

$$G_i(r)=\frac{1}{\rho}\int\delta(r-|\vec{\mathbf{x}}_i-\vec{\mathbf{x}}|)\psi(\vec{\mathbf{x}})d\vec{\mathbf{x}}, \tag{6}$$

where $\rho=(1/A)\int\psi(\vec{\mathbf{x}})d\vec{\mathbf{x}}$ is the domain density, $\vec{\mathbf{x}}_i$ is the position vector of the core center of the domain, and A is the total area for the two-dimensional case.

Considering the whole system with the total number of domains N, the domain-spatial correlation function $G(r)$ is the ensemble average of this number for all core-center positions of over all domains placed at the origin:

$$G(r)=\frac{1}{\rho}\left\langle\sum_{i}^{N}\int\delta(r-|\vec{\mathbf{x}}_i-\vec{\mathbf{x}}|)\psi(\vec{\mathbf{x}})d\vec{\mathbf{x}}\right\rangle. \tag{7}$$

For droplet patterns, in which domains are isolated from each other, the static domain-spatial correlation function has the following properties.

(a) When $r\ll R_{max}$ and R_{max} is the maximum domain size, for any of the domains j, with size R_j, $j=1,2,\ldots,N$, and $r_{ij}=|\vec{\mathbf{x}}_i-\vec{\mathbf{x}}_j|=r$, we get

$$\psi(\vec{\mathbf{x}}_j)=\int\delta(R_j-r)dr=H(R_j-r), \tag{8}$$

$$\delta(r-|\vec{\mathbf{x}}_i-\vec{\mathbf{x}}_j|)=\delta(r-r_{ij})\equiv 1, \tag{9}$$

where $H(R_j-r)$ is the Heaviside step function

$$H(R_j-r)=\begin{cases}1 & \text{if } R_j-r\leq 0\\ 0 & \text{if } R_j-r>0.\end{cases} \tag{10}$$

(i) For a monodisperse (equal-size) droplet pattern with radius R and $r\leq R$, Eq. (7) reduces to

$$G(r)=\frac{1}{\rho}\left\langle\sum_{i,j;i\neq j}^{N}\delta(r-r_{ij})H(R-r)\right\rangle=\frac{1}{\rho}H(R-r). \tag{11}$$

(ii) For a polydisperse droplet pattern with size distribution $f(R)$, which is the probability of a domain having a size between R and $R+dR$, we define the size distribution as $f(R)=N^{-1}\partial N(R)/\partial R$, where $N(R)$ is the number of domains with sizes equal to or larger than R. In this case, Eq. (7) reduces to

$$G(r)=\frac{1}{\rho}\left\langle\sum_{j}^{N}\int\delta(R_j-r)dr\right\rangle=\frac{1}{\rho}\left\langle\sum_{j}^{N}H(R_j-r)\right\rangle=\frac{1}{\rho}\frac{N(R\geq r)}{N}=\frac{1}{\rho}\int_0^r[1-f(R)]dR, \tag{12}$$

where $N(R\geq r)$ is the number of domains with sizes equal to or larger than r. Therefore, $G(r)$ represents the domain-size distribution function when $r<R_{max}$.

(b) When $r\gg R_{max}$, for an arbitrarily chosen domain i with $\vec{\mathbf{x}}_i$ as the origin of the domain core center and $\vec{\mathbf{x}}_j\in$ domain j with radius R_j, $G_i(r)$ of Eq. (3) can be expressed as

$$G_i(r)=\langle\delta(r-|\vec{\mathbf{x}}_i-\vec{\mathbf{x}}_j|)\psi(\vec{\mathbf{x}}_j)\rangle=\left\langle\delta(r-r_{ij})\frac{2\sqrt{R_j^2-(r-r_{ij})^2}dr}{2\pi r\,dr}\right\rangle=\left\langle\delta(r-r_{ij})\frac{\sqrt{R_j^2-(r-r_{ij})^2}}{\pi r}\right\rangle. \tag{13}$$

The domain-spatial correlation function for $r\gg R_{max}$ [Eq. (7)] becomes

$$G(r)=\frac{1}{\rho}\left\langle\sum_{i,j=1;i\neq j}^{N}\delta(r-r_{ij})\frac{\sqrt{R_j^2-(r-r_{ij})^2}}{\pi r}\right\rangle. \tag{14}$$

The term of $(1/\rho)\Sigma\delta(r-r_{ij})$ is actually the pair correlation function of the domain-core centers. The term $\sqrt{R_j^2-(r-r_{ij})^2}/\pi r$ has a maximum value when $r-r_{ij}=0$. Therefore, $G(r)$ represents the spatial correlation function of domains and the peak positions are the same as those of the pair correlation function of the domain-core centers when $r\gg R_{max}$.

III. EVALUATION OF STATIC DOMAIN-SPATIAL CORRELATION FUNCTION

The above discussion clearly conveys the physical meaning and properties of the domain-spatial correlation function. The domain-spatial correlation function simultaneously probes the domain-geometric distribution and the domain-spatial distribution. In order to characterize the experimental data and elucidate the governing scaling relations, the domain-spatial correlation function based on Eq. (4) can be calculated for the total domain-spatial space used in the image analysis:

$$G(r)=\frac{1}{\rho}\left\langle \sum_{i}^{N} \int \delta(r-|\vec{\mathbf{x}}_i-\vec{\mathbf{x}}|)\,\psi(\vec{\mathbf{x}})\,d\vec{\mathbf{x}} \right\rangle \cong \frac{1}{\rho}\left\langle \sum_{i}^{N} \sum_{j}^{N_p} \delta(r-r_{ij})\,\psi(\vec{\mathbf{x}}_j) \right\rangle, \tag{15}$$

where r is the radius of the shell whose center is the core center of an arbitrary growth domain as an origin, $r_{ij}=|\vec{\mathbf{x}}_i-\vec{\mathbf{x}}_j|$, $\vec{\mathbf{x}}_i$ is the position vector of the core center of the growth domain, $\vec{\mathbf{x}}_j$ is the pixel position vector within the growth domain, N is the number of the growth domains in the test area A, and the density ρ is

$$\rho=\frac{1}{A}\int \psi(\vec{\mathbf{x}})\,d\vec{\mathbf{x}} \cong \frac{1}{N_p}\sum_{j}^{N_p} \psi(\vec{\mathbf{x}}_j), \tag{16}$$

where N_p is the total pixel number in the test area A.

Based on Eqs. (15) and (16), we developed image analysis software for computing the time-dependent DSCF directly from experimental images. For the experimental case, the input data are the digitalized coordinates of the core centers of the growth domains and the binary images. The results are based on multiple image sampling and the correction of edge effects. Multiple sampling and the correction of edge effects are standard statistical technique used in stochastic geometry [2] in order to avoid statistical bias.

In order to evaluate this correlation function, we generated images with hypothetical equal-size particles where the spatial distributions are a liquidlike state pattern (see the inset in Fig. 1) or a solidlike state pattern (see the inset in Fig. 2). The characteristic features of the DSCF in Fig. 1 are a broad first peak, a smooth second peak, and a third peak with an appreciably diminished intensity, confirming the complete absence of the long-range order, corresponding to a liquidlike state. The flat part and the sharp drop in intensity close to the left corner of Fig. 1 reflect the equal-size distribution of the particles. Figure 2 shows a DSCF that has pronounced peaks at positions corresponding to a hexagonal-close-packed crystal. A considerably sharper and narrower first peak compared to the liquidlike states, a split in the second peak, and the presence of a distinct third peak in Fig. 2 are the characteristic features of the solid state. Also, the periodic distance in peak positions confirms the long-range order. The flat part and the sharp drop in intensity close to the left corner of Fig. 2 again reflect the equal-size distribution of the particles. The computed results and the features of the DSCF curves agree with Eq. (11).

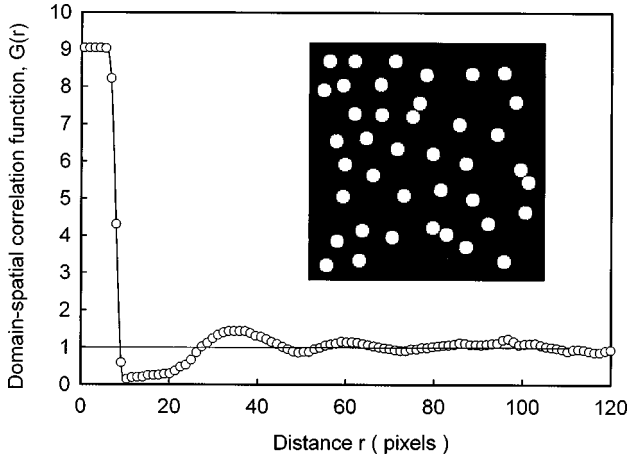

FIG. 1. Domain-spatial correlation function for equal-size particles, where the spatial distributions is a liquidlike state. The flat part and the sharp drop in intensity close to the left corner of the figure reflects the equal-size distribution of the particles. In the spatial correlation part, there is a broad first peak, a smooth second peak, and a third peak with an appreciably diminished intensity, confirming the complete absence of the long-range order corresponding to a liquidlike state.

Figure 3 shows typical results from an experiment involving simultaneous nucleation. It shows growth domains with equal sizes and some local impingement structures with some different-size domains. The DSCF gives a flat part (region 1), which represents the equal-size domains, and the smooth curve (region 2) indicates the domain-size distribution for the local impingement structures. The right-hand side of Fig. 3 represents the pair correlation function of the domain-core centers. It approaches one in an oscillatory manner, with increasing distance.

Figure 4 shows typical results from an experiment of con-

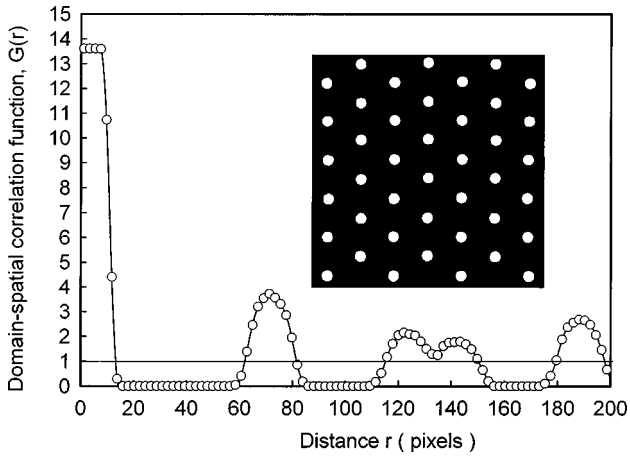

FIG. 2. Domain-spatial correlation function for equal-size particles where the spatial distribution is a solidlike state. The flat part and the sharp drop in intensity close to the left corner of the figure reflects the equal-size distribution of the particles. In the spatial correlation part, there are pronounced peaks at positions corresponding to a hexagonal-close-packed crystal. A considerably sharper and narrower first peak compared to the liquidlike states, a split in the second peak, and the presence of a distinct third peak are the characteristic features of a solid state. Also, the periodic distance in peak positions confirms the long-range order.

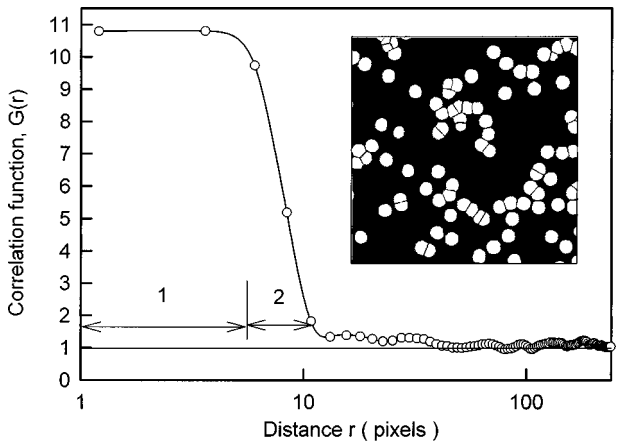

FIG. 3. Typical static domain-spatial correlation function from an experimental image (see the inset) of a simultaneous nucleation case. It shows the growth of domains with equal sizes and some local impingement structures with some different-size domains. The DSCF gives a flat part (region 1), which represents the equal-size domains, and the smooth curve (region 2) indicates the domain-size distribution for the local impingement structures. The right part represents the pair correlation function of the domain-core centers. It approaches one in an oscillatory manner with increasing distance.

tinuous nucleation. The first arrow in Fig. 4 indicates the maximum domain size and the second arrow indicates the first peak of the pair correlation function. The inset in Fig. 4 shows that there are some isolated growth domains with different sizes and some local impingement structures with different domain sizes. The slope of the DSCF for $r \leqslant R_{max}$ reflects the broadness of the domain-size differences.

IV. DYNAMIC DOMAIN-SPATIAL CORRELATION FUNCTION OF NUCLEATION AND GROWTH

The order parameter in the nucleation and growth of polymer systems is the spherulitic growth domain, thus

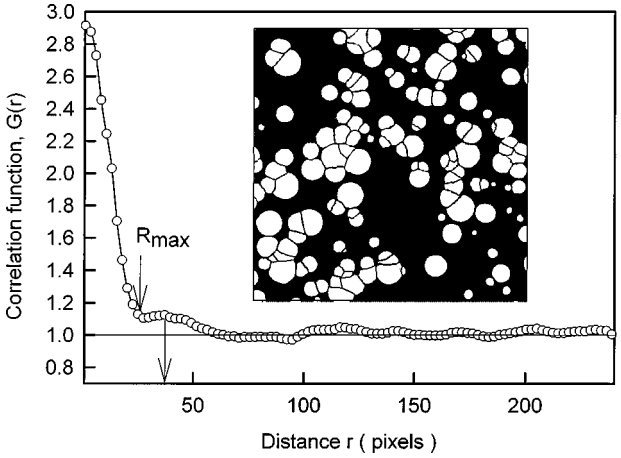

FIG. 4. Typical static domain-spatial correlation function from an experimental image (see the inset) of a continuous nucleation case. The first arrow indicates the maximum domain size and the second arrow indicates the first peak of the pair correlation function. The inset image shows that there are some isolated growth domains with different sizes and some local impingement structures with different-size domains. The slope of the DSCF for $r \leqslant R_{max}$ reflects the broadness of the domain-size differences.

$$\psi(\vec{\mathbf{x}},t)=\begin{cases}1 & \text{if } \vec{\mathbf{x}} \in \text{the spherulitic domain at time } t\\ 0 & \text{if } \vec{\mathbf{x}} \in \text{the melt at time } t.\end{cases} \tag{17}$$

Sekimoto indicated that $\psi(\vec{\mathbf{x}},t)$ is connected with the volume fraction of the stable crystallized phase $\chi(t)$ in KJMA's formula [5], which reads [14]

$$\langle \psi(\vec{\mathbf{x}},t)\rangle = 1-\chi(t)=\begin{cases}\exp\left[-\int_0^t dt\ I(t)\Psi(t)\right] \\ \qquad \text{for } V(t) \text{ and } I(t) \\ \exp(-IC_dV^dt^{d+1}) \\ \qquad \text{for constant } V \text{ and } I,\end{cases} \tag{18}$$

where d is the spatial dimensionality, $C_1=1$, $C_2=C_3=\pi/3$, I is the nucleation rate, V is the growth velocity, and $\Psi(t)$ is the volume of the d-dimensional unit hypersphere.

According to Eq. (5), the domain-spatial correlation function can be expressed as

$$G(r,t)=\left[\frac{1-\chi(t)}{\Re}\right]^{-1}\left\langle \sum_{i=1}^{N}\int \delta(r-|\vec{\mathbf{x}}_i-\vec{\mathbf{x}}|,t)\,\psi(\vec{\mathbf{x}},t)\,d\vec{\mathbf{x}}\right\rangle, \tag{19}$$

where $\Re$ is the geometric measure of the test region. Therefore, the domain-spatial correlation function for nucleation and growth provides complete information of the transformed volume fraction, the time-dependent domain-size distribution function, and the spatial correlation function of domain-core centers simultaneously.

V. EXPERIMENTAL RESULTS AND DISCUSSION

Experiments on nucleation and growth in two-dimensional semicrystalline polymer films during free solidification were carried out with isotatic polyporpylene (molecular weight $M_\eta = 250\,000$). A polymer thin film was formed between two glass slides while pressing the top slide to form a 10-μm-thick polymer film. A Leitz polarizing microscope, equipped with a Leitz hot stage for polymer film solidification, was used in the direct observation experiments. In this isothermal solidification study, the temperature is controlled within ± 0.1 °C. JAVA-Jandel Scientific's video measurement and image processing system was directly connected to the microscope via a charge coupled device camera. We use commercial software, Visilog 5.02 (from Noesis Vision Inc., Québec), for basic image processing. We focus on the postnucleation stage, during which the size of the nuclei is greater than 1 μm and visible under the optical microscope for real-time *in situ* observation and accurate real-space measurements. We present the experimental results in terms of the time-dependent DSCF. The DSCF $G(r,t)$ is plotted as a function of distance r for different nucleation cases. The growth velocity under isothermal crystallization conditions is constant for semicrystalline polymers. Actually, the nucleation rate and growth velocity depend on the system melt properties, thermal history, and crystallization conditions. The nucleation in semicrystalline

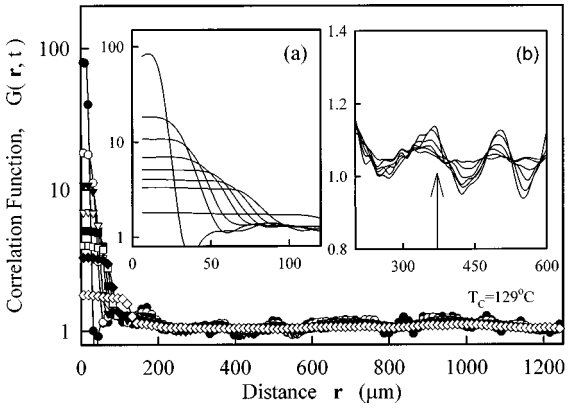

FIG. 5. Dynamic domain-spatial correlation function from the simultaneous nucleation experiment under isothermal crystallization temperature $T_c = 129$ °C. Inset (a) is the size distribution and (b) is the spatial correlation.

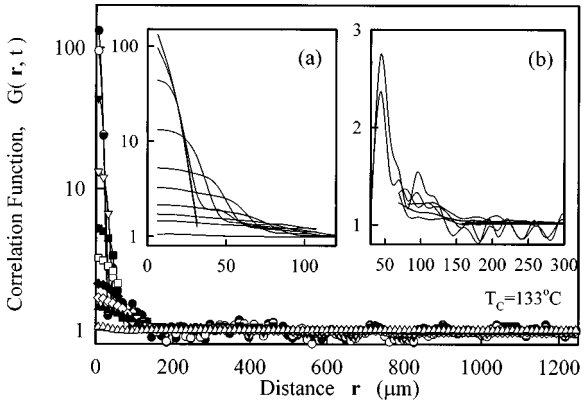

FIG. 7. Dynamic domain-spatial correlation function from the continuous nucleation experiment under isothermal crystallization temperature $T_c = 133$ °C. Inset (a) is the size distribution and (b) is the spatial correlation.

polymers can be categorized as (i) simultaneous nucleation, (ii) continuous nucleation, and (iii) multistep nucleation.

A. Simultaneous nucleation

Figures 5 and 6 show the time-dependent DSCF $G(r,t)$ plotted as a function of the distance r for two sets of typical experimental data involving the simultaneous nucleation case at two different crystallization temperatures. In both figures inset (a) shows the spherulite domain size distribution and (b) shows the radial distribution.

In the simultaneous nucleation case, polymer crystallization involves a constant growth velocity V. The spatial distribution of nucleation sites can be of any kind, but timewise it is unique. The nucleation growth has an instantaneous site saturation. The nucleation rate is

$$I(t) = I_0 \delta(t - t_I), \tag{20}$$

where I_0 is the constant nuclei density, t_I is the induction time, and $\delta(t-t_I)$ is the Dirac delta function.

For $r \leqslant R(t)$ and before impingement, the domain-spatial correlation function [Eq. (19) with Eq. (11)] becomes

$$G(r,t) = \left[\frac{1-\chi(t)}{A}\right]^{-1} \left\langle \sum_{i,j;i\neq j}^{N} \delta(r - r_{ij}) H(R_j - r) \right\rangle$$
$$= \left[\frac{\exp\left(-\frac{\pi}{3} I_0 V^2 t^3\right)}{A}\right]^{-1} H(Vt - r). \tag{21}$$

Thus, in the free growth stage, $G(r,t)$ is a step function with a width of Vt and the height of $G(r,t)$ decreases with increasing time. After impingement, there is a mixture of isolated spherulitic domains and some impinged grain islands; $G(r,t)$ is a step function representing the equal-size spherulitic domains. It is connected with a smooth oblique curve that decreases with increasing r, representing the domain-size variation due to impingement.

The experimental results agree with the above analysis very well. The major features of the DSCF are that $G(r=0,t)$ decrease as time increase, which reflects the increase in transformed area; for $r \leqslant R_{max}(t)$, the lower r flat section of the DSCF becomes larger because of the growth of spherulitic domains; and for $r \gg R_{max}(t)$, the positions of the first peak, the average interdomain center distance, remain

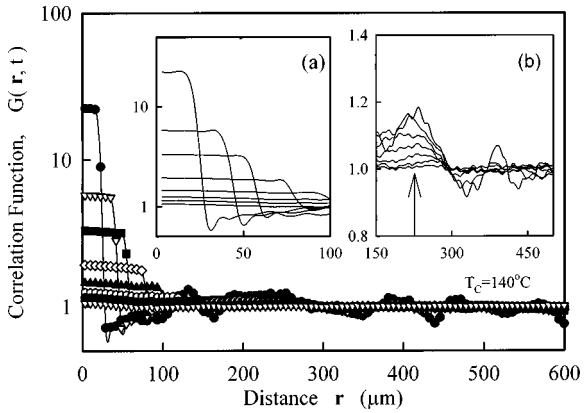

FIG. 6. Dynamic domain-spatial correlation function from the simultaneous nucleation experiment under isothermal crystallization temperature $T_c = 140$ °C. Inset (a) is the size distribution and (b) is the spatial correlation.

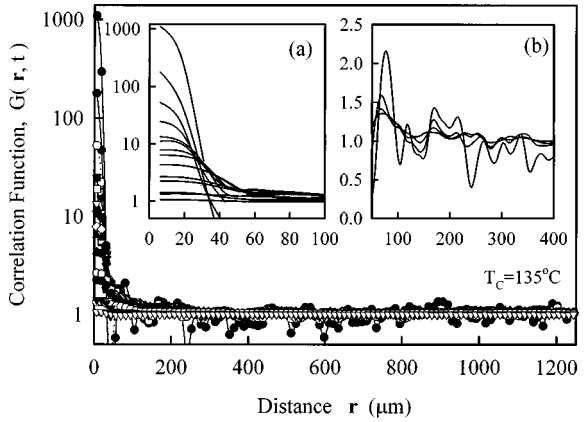

FIG. 8. Dynamic domain-spatial correlation function from the continuous nucleation experiment under isothermal crystallization temperature $T_c = 129$ °C. Inset (a) is the size distribution and (b) is the spatial correlation.

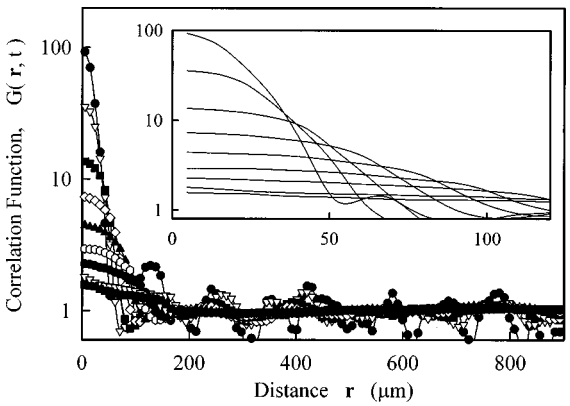

FIG. 9. Dynamic domain-spatial correlation function from the continuous nucleation experiment under isothermal crystallization temperature $T_c = 137$ °C and the inset size distribution.

unchanged because there are no new domains formed during the domain growth process in the simultaneous nucleation case. $G(r,t)$ approaches one in an oscillatory manner at very large r, which means that there is no long-range order. The time-dependent DSCF $G(r,t)$ smoothly captures the entire process, including the postnucleation, domain growth, and grain formation stages. The DSCF directly and simultaneously explores the transformed volume fraction, the time-dependent domain-size distribution, and the spatial correlation of domain-core centers throughout the entire process.

B. Continuous nucleation

Under continuous nucleation, the growth velocity V is constant during polymer isothermal crystallization. The spatiotemporal distributions of nucleation sites are of various types. From experimental measurements [20], a nearly linear nucleation law is found after an induction period. The nucleation rate $I(t)$ can be described by Kashchiev's nucleation kinetics [21], which is given as

$$\frac{I(t)}{I_0} = \left\{ 1 + 2\sum_{n=1}^{\infty} (-1)^n \exp\left[-n^2 \left(\frac{t}{t_I} \right) \right] \right\}, \qquad (22)$$

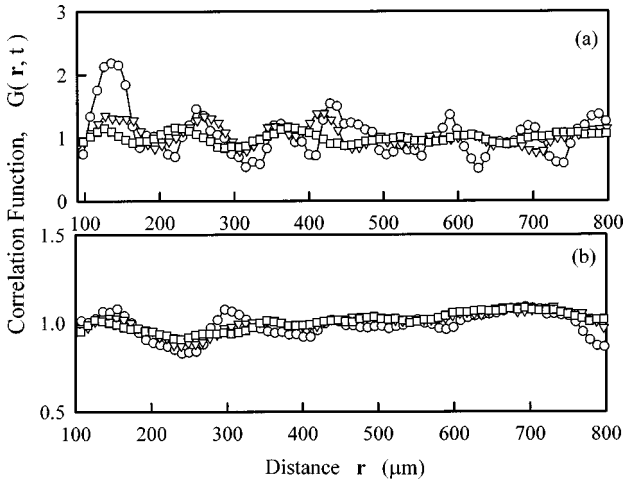

FIG. 10. Spatial correlation function part of the dynamic domain-spatial correlation function in Fig. 9: (a) early stage and (b) late stage.

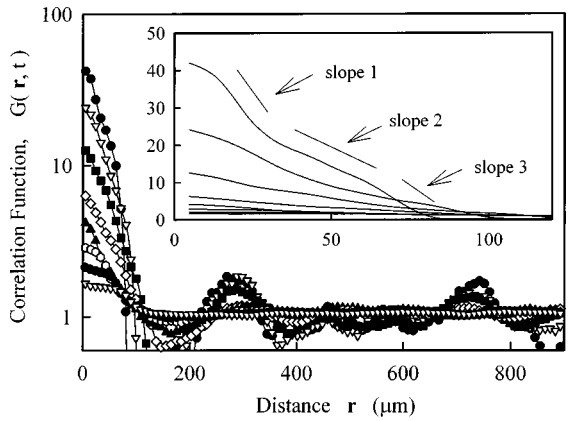

FIG. 11. Dynamic domain-spatial correlation function from a typical multiple nucleation experiment; the inset is the size distribution.

where t_I is an induction time. The initial nucleation rate should be very high, but it soon decays to the linear steady-state value. Experimental observations show that the linear steady nucleation rate decreases to zero when impingement becomes significant with increasing transformation. For $r \leq R_{max}(t)$ before impingement, the domain-spatial correlation function (19) becomes

$$G(r,t) = \left[\frac{\exp\left(-\frac{\pi}{3} I V^2 t^3 \right)}{A} \right]^{-1} \int_0^r [1 - f(R,t)]\, dR. \qquad (23)$$

Figures 7 and 8 show the time-dependent DSCF $G(r,t)$ as a function of distance r for two sets of typical experimental data involving the simultaneous nucleation case. Inset (a) is a zoom of the smooth curves of the domain size distribution when $r \leq R(t) = Vt$, where $R(t)$ is the domain size and V is the growth velocity. It represents the growth of domains with different sizes and some local impingement structures. Inset (b) is the zoom of the spatial pair correlation function of domain-core centers when $r > R(t) = Vt$. The first peak slightly shifts to the left with increasing time, which means

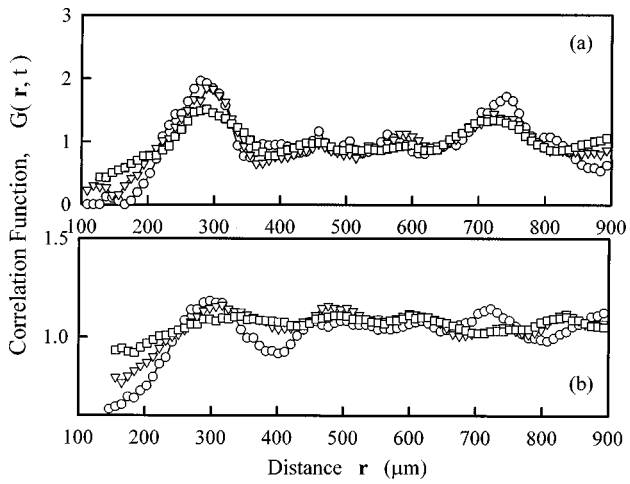

FIG. 12. Spatial correlation function part of the dynamic domain-spatial correlation function in Fig. 11: (a) early stage and (b) late stage.

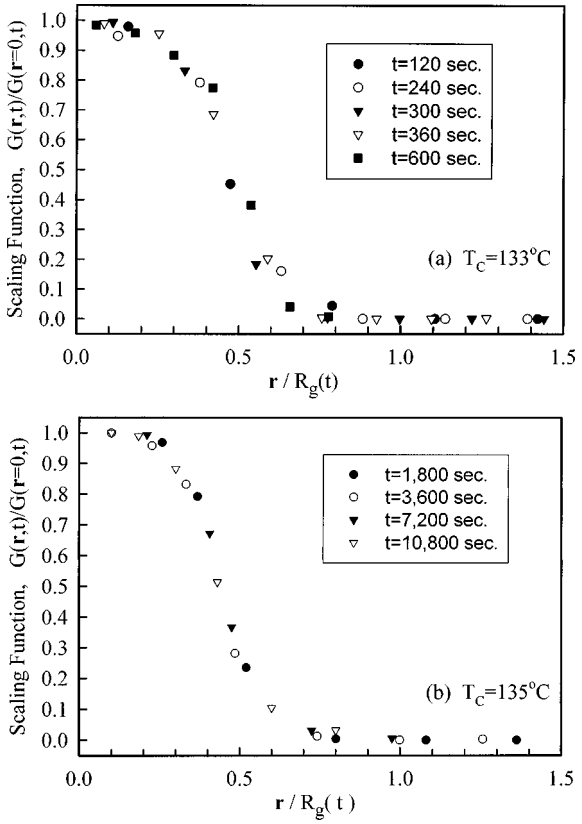

FIG. 13. Experimental results of the scaling relation $G(r,t)/G(r=0,t)$ as a function of $r/R_g(t)$ from the continuous nucleation experiment at isothermal temperatures (a) $T_C=133$ °C and (b) $T_C=133$ °C, respectively.

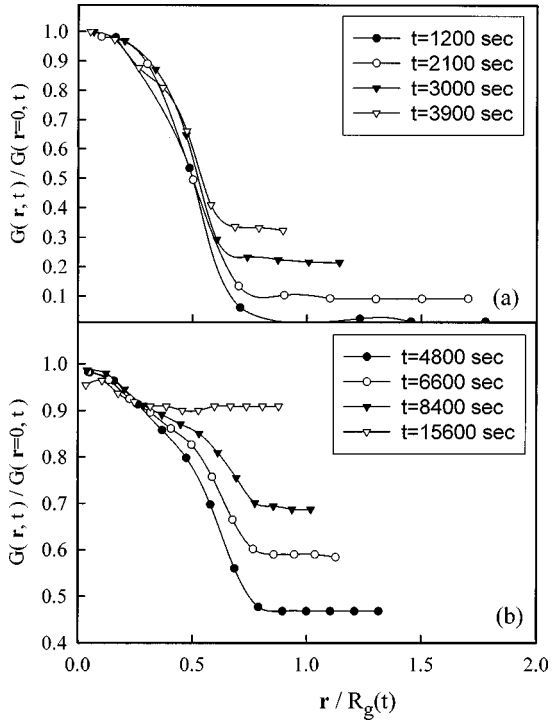

FIG. 14. Experimental results of the scaled correlation function $G(r,t)/G(r=0,t)$ as a function of $r/R_g(t)$ in an isothermal experiment, at $T_c=133$ °C. (a) Growth and impingement with a transformed fraction less than 0.5; the scaling relations are partially obeyed. (b) Growth and impingement with a transformed fraction greater than 0.5; the scaling relations break down in the late stages of growth.

that the average internuclei distances decrease with time. However, the peak stops shifting in later stages. $G(r,t)$ approaches one in an oscillatory manner at very large r, which means that there is no long-range order.

Figure 9 shows more distinctively the same DSCF features in another isothermal experiment at $T_c=137$ °C. The inset in Fig. 9 shows the smooth curves of domain-size distributions. Figure 10(a) shows the spatial pair correlation function of domain-core centers as a function of r at an earlier stage and Fig. 10(b) shows that at a later stage, corresponding to Fig. 9. These plots show that the average core distances, the first peak positions, decrease with time.

C. Multiple nucleation

In multiple nucleation, it is assumed that nucleation occurs by a series of elementary steps. The nucleation rate can be written as

$$dn/dt=k_{i-1}n_{i-1}-k_in_i \tag{24}$$

for $i=1,2,\ldots$, $dn_0/dt=k_0n_0$. When $k_it\ll 1$, $n=kt^p$. The small step changes in crystallization temperature will strongly affect the nucleation rate; however, the growth velocity does not exhibit significant changes. Figure 11 shows the experimental results of the DSCF for multiple step nucleation. Figure 12(a) shows the spatial pair correlation function of domain-core centers as a function of r at an early stage and Fig. 12(b) shows that at a later stage, corresponding to Fig. 10. These plots show that the average core distances, the first peak positions, decrease with time. Figure 11 shows clear changes in the slopes of the domain-size distribution (see the inset in Fig. 11).

For early free growth stage, the size distribution can be expressed as

$$f(R,t)=\frac{1}{N}\frac{\partial N(R,t)}{\partial R}=\frac{I[t^*(R)-t]}{\int_0^R I[t^*(R)-t]dR}, \tag{25}$$

where $I[t^*(R)-t]$ is nucleation rate and $t^*(R)=R/V$. Then we find that the slope of $G(r,t)$ is related to the nucleation rate when $r\ll R_{max}$ as

$$\frac{\partial G(r,t)}{\partial r}=\frac{-I[t^*(R)-t]}{\{A[1-\chi(t)]\}^{-1}\int_0^R I[t^*(R)-t]dR}$$

$$=\frac{-1}{N(t)}I[t^*(R)-t]. \tag{26}$$

According to Eq. (26), a slope change in the DSCF indicates a step change in the nucleation rate. In Fig. 10 $I_1>I_3>I_2$ is shown as slopes 1, 2, and 3. The smaller the slope on the DSCF, the smaller the nucleation rate and also the broader the domain-size distribution.

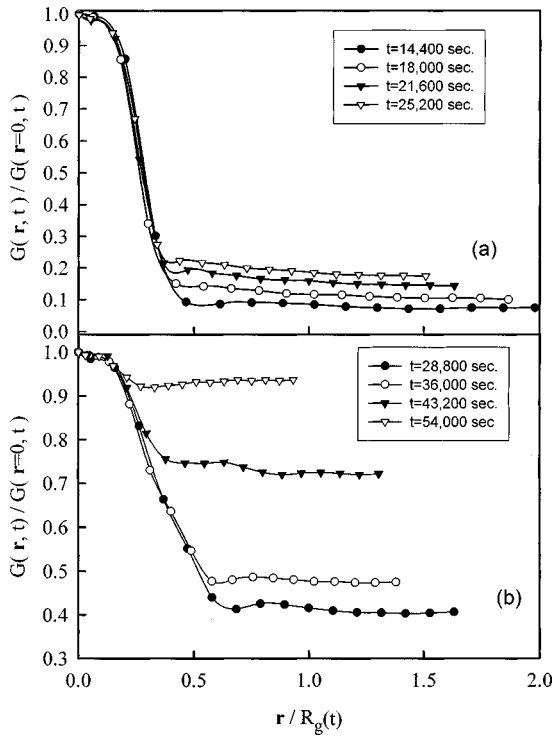

FIG. 15. Experimental results of the scaling correlation function $G(r,t)/G(r=0,t)$ as a function of $r/R_g(t)$ in an isothermal experiment at $T_c=135$ °C. (a) Growth and impingement with a transformed fraction less than 0.5; the scaling relations are partially obeyed. (b) Growth and impingement with a transformed fraction greater than 0.5; the scaling relations break down in the late stages of growth.

D. Scaling relation for free growth

A scaling relation of domain-spatial correlation functions may be written in the form that was used for the pair correlation function in phase separation studies [22–25]:

$$G(r,t)\cong G(0,t)\mathcal{G}(r/R_g(t)) \quad \text{for } \epsilon\ll r\ll L, \tag{27}$$

where ϵ is some lower bound on the sizes of any domain in the system, L is the linear size of the system, and $R_g(t)$ is the location of the first minimum of $G(r,t)$. $G(0,t)$ is understood to be some limiting value of $G(r,t)$ when r is of order ϵ. The scaling function $\mathcal{G}(r/R_g(t))$ is independent of time.

Figure 13 presents the scaling from the experimental results of the normalized correlation functions $G(r,t)/G(r=0,t)$ as a function of $r/R_g(t)$ for the early free growth stage for two different crystallization temperatures $T_c=133$ °C and $T_c=135$ °C. In both cases, experimental results are superimposed on one curve and thus confirm the scaling relation of the correlation functions for the early free growth during the postnucleation stage. This result for a two-dimensional system agrees with Axe and Yamada's [16] analytical results in a one-dimensional system.

E. Scaling and impingement

Figures 14 and 15 show the experimental results of the scaling correlation function $G(r,t)/G(r=0,t)$ as a function of $r/R_g(t)$: (a) shows the case for growth and impingement when the transformed fraction is less than 0.5, where the scaling relations are partially obeyed and (b) shows the case for growth and impingement when the transformed fraction is greater than 0.5. The scaling part indicates the percentage of the unimpinged domain. The scaling relations break down in the late stages of growth and for grain structures due to impingement. Figure 16 suggests a linear evolution of the scaling function as a function of time, following the breakdown of the scaling during the impingement process. This relation is supported by all of the experimental results and appears to be universal. It could provide an approach for interpolation between the impingement stage and grain structures. In addition to the above application, the domain-spatial correlation function and the direct imaging program are suitable to characterize any static droplet patterns and dynamic processes in a wide range of scientific fields.

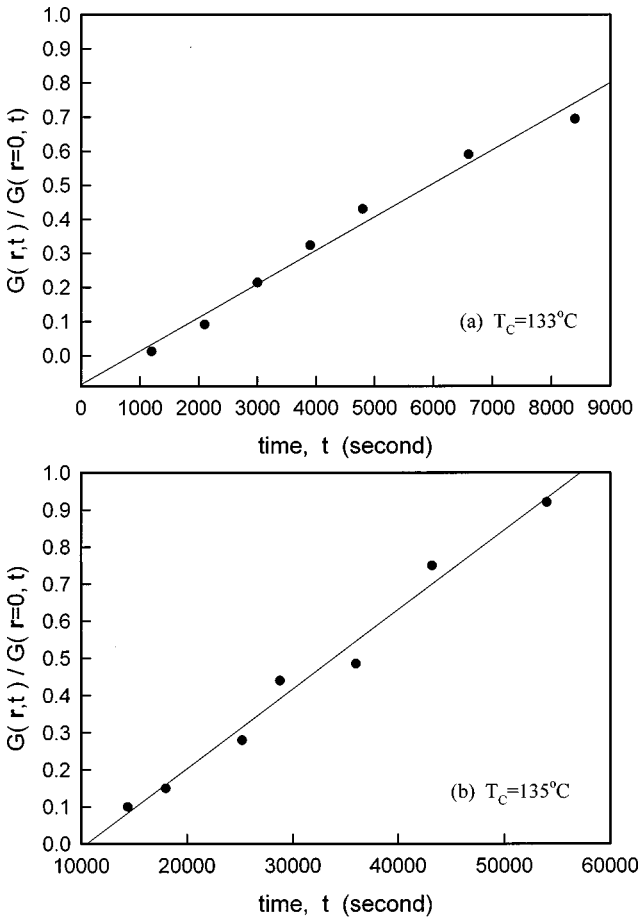

FIG. 16. Experimental results of the scaled correlation function $G(r,t)/G(r=0,t)$ as a function of the time of the breakdown of the scaling during the impingement processing: (a) $T_C=133$ °C and (b) $T_C=133$ °C, respectively.

VI. CONCLUSION

We present an approach on postnucleation and domain growth in term of a domain-spatial correlation function $G(r,t)$. It probes the patterns and spatiotemporal evolution of nucleation and growth processes and agrees very well with experimental data. The dynamic domain-spatial correlation function directly and simultaneously explores the transformed volume fraction, the time-dependent domain-size distribution function, and the spatial correlation function

of domain-core centers for the entire process, including the postnucleation, domain growth, and grain formation stages. The scaling relation $\mathcal{G}(r/R_g(t))=G(r,t)/G(r=0,t)$ has been found from experimental data, where $R_g(t)$ is the location of the first minimum of $G(r,t)$. It is exact for free growth during the postnucleation stage and also suggests a basis for interpolation between the impingement stage and grain structures.

[1] J. W. Evans, Rev. Mod. Phys. **65**, 1281 (1993), and references therein.

[2] D. Stoyan and W. S. Kendall, *Stochastic Geometry and Its Applications* (Wiley, New York, 1995).

[3] J. D. Gunton, M. San Miguel, and P. Sahni, in *Phase Transitions and Critical Phenomena*, edited by C. Domb and J. L. Lebowitz (Academic, London, 1983), Vol. 8, p. 267; J. D. Gunton and M. Droz, *Introduction to the Theory of Metastable and Unstable States* (Springer-Verlag, Berlin, 1983).

[4] A. J. Bray, Adv. Phys. **43**, 357 (1994).

[5] A. N. Kolmogorov, Bull. Acad. Sci. USSR, Phys. Ser. **1**, 355 (1937); W. Johnson and R. F. Mehl, Trans. Am. Inst. Min. Metall. Pet. Eng. **135**, 416 (1939); M. Avrami, J. Chem. Phys. **7**, 1103 (1939); **8**, 212 (1940); **9**, 177 (1941).

[6] J. S. Langer, in *Solids Far From Equilibrium*, edited by C. Godréche (Cambridge University Press, Cambridge, 1989), Chap. 3, p. 297.

[7] J. S. Langer and A. J. Schwartz, Phys. Rev. A **21**, 948 (1980).

[8] K. Binder and D. Stauffer, Adv. Phys. **25**, 343 (1976).

[9] S. Krishnamurthi and W. I. Goldburg, Phys. Rev. A **22**, 2147 (1980).

[10] A. Cumming, P. Wiltzius, F. S. Bates, and J. H. Rosedale, Phys. Rev. A **45**, 885 (1992).

[11] K. Schatzel and B. J. Ackerson, Phys. Rev. E **48**, 3766 (1993).

[12] N. P. Balsara, Chenchy Lin, and B. Hammouda, Phys. Rev. Lett. **77**, 3847 (1996).

[13] B. Morin, K. R. Elder, M. Sutton, and M. Grant, Phys. Rev. Lett. **75**, 2156 (1995); B. Morin, Ph.D. thesis, McGill University, 1993 (unpublished).

[14] K. Sekimoto, Phys. Lett. **105A**, 390 (1984); J. Phys. Soc. Jpn. **53**, 2425 (1984); Physica A **137**, 96 (1986).

[15] S. Ohta, T. Ohta, and K. Kawasaki, Physica A **140**, 478 (1987).

[16] J. D. Axe and Y. Yamada, Phys. Rev. B **34**, 1599 (1986).

[17] Tao Huang, A. D. Rey, and M. R. Kamal, Polymer **25**, 5434 (1994).

[18] Tao Huang, Tomohiro Tsuji, M. R. Kamal, and A. D. Rey, Phys. Rev. E **58**, 789 (1998).

[19] J. P. Hansen and I. R. McDonald, *Theory of Simple Liquids* (Academic, New York, 1986).

[20] Tao Huang, A. D. Rey, and M. R. Kamal, Macromolecules **31**, 1218 (1998).

[21] D. Kashchiev, Surf. Science **14**, 209 (1969).

[22] R. Toral, A. Chakrabarti, and J. D. Gunton, Phys. Rev. B **39**, 901 (1989).

[23] T. M. Rogers and R. C. Desai, Phys. Rev. B **39**, 11 956 (1989).

[24] K. R. Elder and R. C. Desai, Phys. Rev. B **40**, 243 (1989).

[25] P. Fratzl, J. L. Lebowitz, O. Penrose, and J. Amar, Phys. Rev. B **44**, 4794 (1991).